

Entanglement Relaxation and Release in Hard Chain Fluids during Molecular Dynamics Simulations

Julie A. McCormick, Carol K. Hall,* and Saad A. Khan

Department of Chemical Engineering, Box 7905, North Carolina State University, Raleigh, North Carolina 27695-7905

Received July 2, 2001; Revised Manuscript Received May 2, 2002

ABSTRACT: Discontinuous molecular dynamics simulations are performed on systems containing 32 hard chains of length 192 at three volume fractions, $\phi = 0.40, 0.45,$ and $0.50,$ to investigate entanglement relaxation and release in model polymer melts. The relaxation behavior of the systems is compared to that predicted by the tube model and to that suggested for the release of interchain entanglements, or knots. The mean squared displacement of the chain center of mass, the mean squared displacements of inner, outer, and intermediate segments along the chain, the end-to-end vector autocorrelation function, and the apparent self-diffusion coefficient are calculated over the course of the simulations. The three relaxation times ($\tau_e,$ $\tau_R,$ and τ_d) predicted by the tube model are estimated in order to determine the extent to which the results exhibit tube confinement. The initial relaxation of chain segments occurs from the ends toward the middle as the tube model predicts. However, different methods for predicting the longest relaxation time, $\tau_d,$ provide inconsistent results. An analysis of the mean squared displacement behavior of chain segments at various positions along the chain reveals when final relaxation occurs and suggests that the final relaxation is occurring at the chain ends, inconsistent with the tube model but compatible with the release of interchain entanglements or knots. A combined analysis of the end-to-end vector autocorrelation function, the outer segment mean squared displacement, and the apparent diffusion coefficient suggests that knot release behavior is occurring in the systems. The results provide support for a proposed mechanism of interchain entanglement relaxation consisting of initial relaxation, followed by memory and final release from a chain end; however, the uncertainty is large at these long times.

I. Introduction

Despite the abundance of experimental correlations for polymers, the link between the microscopic behavior of polymer molecules and their dynamic properties is not completely understood. To ascertain how a polymer's microscopic structure, and hence its macroscopic mechanical properties, evolve during processing, it is essential to determine how polymers move in a melt. This motion is complicated by the presence of entanglements, which create a spectrum of time scales and strongly influence the dynamic properties that are observed macroscopically, such as the self-diffusion coefficient and viscosity. Although the presence of entanglements is widely accepted, the exact nature of entanglements is not known.¹ The microscopic origin of entanglements and the details of their microscopic motion, including the mechanism of their relaxation and release, have been the subject of debate.

At least two different approaches can be used to describe the nature of polymer entanglements,^{1,2} and hence entanglement relaxation and release. These approaches differ in their method of describing entanglements. The first approach reduces the multichain problem to that of a single chain in a mean field, while the second approach emphasizes the existence of specific interchain entanglements. Reptation³ and the tube model,⁴ examples of the first approach, say that the reptative motion of a polymer chain is slowed by a confining tube of entanglements. Local knot theory^{5,6} and double reptation,^{7–10} examples of the second approach, say that the motion of a polymer chain is restricted by specific, localized entanglements, or knots,

formed with other chains. These theories also give different descriptions for the mechanism of entanglement release. Reptation and the tube model suggest that entanglements in the form of tube confinement relax from the chain ends toward the chain middle. Local knot theory and double reptation say that entanglements will only be released when a chain end moves through a knot. Observing the mechanism of entanglement release provides a means for testing the two theories' ability to describe polymer dynamics.

The aim of this research is to investigate the molecular mechanisms underlying entanglement relaxation and release in model polymer melts using discontinuous molecular dynamics simulations. As far as we know, this is the most comprehensive study to investigate both tube model and local knot ideas simultaneously. This study was inspired, in part, by previous work in which Smith, Hall, and Freeman¹¹ observed evidence of intermolecular knot formation and release in simulations of entangled hard-chain fluids. In an effort to examine their observations in greater detail, we have performed more extensive simulations which span longer times and explore higher densities. We compare the results from these simulations of hard-chain fluids to entanglement relaxation and release predictions of the tube model and to mechanisms hypothesized for interchain entanglement, or knot, release. We calculate the mean squared displacement of segments at different positions along the chain to determine how segment position affects relaxation.

Many studies, both experimental^{12–14} and computational,^{11,15–26} have focused on testing the validity of Doi and Edwards' tube model,^{4,27} the most widely cited theory of polymer dynamics. In the tube model, a melt of entangled polymers is modeled as a single chain moving by

* To whom correspondence should be addressed.

reptation³ through a tube created by the surrounding polymers; specific interchain contacts are ignored, thus simplifying the problem substantially. The tube model²⁷ predicts that the self-diffusion coefficient, D , and viscosity, η , of a fluid containing long entangled chains of length n scale as $D \sim n^{-2}$ and $\eta \sim n^3$ for chains longer than the entanglement length, N_e . These predictions are not rigorously consistent with experimental observations, however, since $\eta \sim n^{3.4}$,²⁸ and $D \sim n^x$ where $-2.3 \leq x \leq -2.0$.^{29,30} In an effort to understand the discrepancy between tube model predictions and experimental results, investigators have examined those aspects of the tube model's description of molecular motion that critically impact the model's macroscopic property predictions.

Information about polymer diffusion is obtained by analyzing the time dependence of chain and chain-segment displacements. The tube model^{4,27} predicts that a single chain confined to a tube exhibits four distinct types of motion as characterized by the scaling of the atomic mean squared displacement, $g(t)$, with time. These four different types of motion are as follows: (1) $g \sim t^{1/2}$ for $t < \tau_e$ where τ_e , the entanglement time, is the time it takes for the chain to discover its confinement to a tube in the lateral direction; (2) $g \sim t^{1/4}$ for $\tau_e < t < \tau_R$ where τ_R , the Rouse time, is the time it takes for the chain to relax within the tube; (3) $g \sim t^{1/2}$ for $\tau_R < t < \tau_d$ where τ_d , the disengagement time, is the time needed for the chain to "disengage," or diffuse, from the tube; and (4) $g \sim t$ for $t > \tau_d$, the so-called free diffusion limit. These four scaling regimes are bound by the three different relaxation times, τ_e , τ_R , and τ_d , each of which denotes a change in dynamic behavior.

Computer simulations yield detailed information about molecular motion and hence are ideally suited for testing theories that are molecularly based like those discussed in this paper. For this reason, a number of research groups have performed extensive simulations of entangled polymer melts^{11,15-26,31-34,2} using one of two different approaches to the problem, either searching for evidence of tube confinement or searching for evidence of specific interchain contacts. The majority of simulations of entangled polymer melts have taken the first approach in an attempt to either prove or disprove the existence of tube confinement.^{11,15-26} This was done by determining the scaling behavior of the self-diffusion coefficient, D , with chain length and the scaling behavior of its underlying microscopic property, the mean squared displacement, $g(t)$, with time.

Most of the early computer simulations of polymer melts were lattice-based Monte Carlo (MC) simulations.¹⁵⁻¹⁸ Skolnick and co-workers¹⁵⁻¹⁸ performed Monte Carlo simulations of decreased long chains (up to $n = 800$) confined to a cubic lattice. The mobility of their chains decreased with increasing chain length as predicted in the tube model. They believed that this decreased mobility indicated the beginning of highly constrained motion, but not necessarily confinement to a tube as the tube model predicts.^{18,35}

The bond fluctuation model has been used to obtain more realistic lattice systems.^{19,21} Paul et al.¹⁹ performed Monte Carlo simulations of long ($n = 200$) chain molecules confined to a cubic lattice. Their bond fluctuation model for the highest occupation fraction they studied ($\phi = 0.5$) provided evidence of reptation. This work was extended by Kreer et al.²¹ to include longer chains up to $N = 512$ in an effort to examine entangle-

ment dominated dynamics. However, they were still unable to observe the asymptotic power laws of the tube model, indicating that even longer chain lengths might be needed.

More extensive and realistic simulations were performed using molecular dynamics (MD). Molecular dynamics simulations of polymer motion offer the advantages that excluded volume is treated more realistically than in lattice models, and the dynamics evolve more naturally than in Monte Carlo simulations. Kremer and Grest²² used Cray vector computers to perform the first molecular dynamics simulations of entangled polymers ($n = 200$) modeled as chains of truncated Lennard-Jones spheres over time scales that covered up to $4^{1/2}$ orders of magnitude in reduced time. They sampled the first two scaling regimes of $g(t)$ behavior but were unable to observe the third and fourth scaling regimes. Like Skolnick and co-workers, Kremer and Grest monitored the mean squared displacement down the tube path and perpendicular to the tube. They found that the chains experienced preferential motion along the tube path, contradicting the conclusion of Skolnick and co-workers.

The simulations of Kremer and Grest²² were later extended to include longer times and longer chains.^{23,24} In the first extension, Dünweg et al.²³ simulated systems of chains with lengths up to $n = 350$ over more than 5 orders of magnitude in reduced time. For chains with $n \leq 200$, this was sufficient to reach free diffusion; however, for the chains of length $n = 350$, they were only able to access the second time regime. They were not able to determine whether the tube model^{4,27} or mode coupling theory^{36,37} provided a better prediction for the scaling behavior. In a subsequent extension, Pütz et al.²⁴ performed simulations on systems containing chains of length $n = 350$, 700, and 10000 in an effort to compare different methods for determining the entanglement length, N_e . The $n = 350$ simulations were extended to 6 orders of magnitude in reduced time, reaching a crossover to free diffusion. (The final relaxation time was not determined however.) The other systems, $n = 700$ and $n = 10\,000$, were simulated only into the second time regime. They found that the different methods for estimating the entanglement length, N_e , (using either the mean squared displacements or the plateau modulus) gave results that differed by a factor of 2.3. This inconsistency may be just a result of incorrect reptation model prefactors instead of a failure of the single chain picture to capture the essential physics of entanglement behavior.

Some of the simulations of entangled polymer melts have taken the second approach, focusing on the search for entanglements in the form of long-lived intermolecular contacts.^{31-34,2} In these studies, computer simulations were used to search for all interchain contacts and then to distinguish truly long-lived entanglements from incidental contacts. The different studies use various methods to do this.

Ben-Naim et al.³⁴ found that incidental contacts appear, disappear, and reappear anywhere along the chain, but true, long-lived entanglements are released only when they reach a chain end. In their study, they performed simulations of 200 chains of length $n = 350$ interacting via a repulsive Lennard-Jones potential with an anharmonic springlike interaction between bonded spheres.²² To visualize monomer contacts between pairs of chains, they formed a "contact map" which is a matrix

whose elements $n(i, j)$ indicate when two monomers, i and j , form a contact ($n(i, j) = 1$) and when they do not ($n(i, j) = 0$). Clustering appeared in small regions on the contact maps; some of these clusters persisted in time, while others appeared and disappeared continuously. A sequence of contact maps were stacked to form three-dimensional maps of contact density $n(i, j, t)$. In these 3-D maps, entanglements appeared as rope-like structures which persisted in time until they were able to diffuse to a chain end where they could be released. Their results revealed that 50% of the contacts between entangled chains are persistent contacts which do not exist in independently moving, unentangled chains.

Smith et al.¹¹ observed evidence for intermolecular knots during their search for tube confinement in entangled chain fluids. They applied highly efficient discontinuous molecular dynamics (DMD) simulation algorithms³⁸ to the simplest possible continuous-space model of a polymer molecule, the hard-chain model. Using this fast technique, they performed long MD simulations^{25,11} spanning $\sim 5^{1/2}$ orders of magnitude in reduced time on systems containing 32 hard chains of lengths ranging from $n = 8$ to $n = 192$ at volume fractions $\phi = 0.30, 0.40,$ and 0.45 . For the 192mers at a volume fraction $\phi = 0.40$, they believed that they were able to observe the transition to the fourth scaling regime for $g(t)$, as predicted in the tube model. However, during the second scaling regime, the chains' mobility was greater than that predicted in the tube model, indicating that the systems studied may not have been entangled enough to reach the scaling limits predicted in the tube model. For the 192mers at $\phi = 0.45$, reduced mobility even closer to that predicted by the tube model was observed, but only three time regimes were sampled despite the long times reached.

One of the most intriguing aspects of Smith et al.'s work¹¹ was the observation of plateaus in the inner segment mean squared displacement, $g(t) \sim t^0$, at long times for 192mers at volume fractions of 0.40 and 0.45. These plateaus were interpreted as evidence for the existence of intermolecular knot formation, based on visualization and analysis of individual chain motion. Immediately following these plateaus was a region of accelerated displacement, $g \sim t^{1.2}$, which was interpreted as a recoil of stored entropic energy in the inner segments that had been stretched during knot disengagement. The discovery of two "knotted" chains, a pair of chains with a distinct topological obstacle to diffusion, through visualization techniques provided evidence for knot formation and release. Because the plateaus and accelerated displacement appeared near the end of the correlation time where the statistics are not as good, the importance of these phenomena, by themselves, is subject to question.^{39,40} Increased averaging from simulations which cover longer times or include more chains may cause the anomalies to average out even if knot formation and release were present. Nevertheless, when one considers the supporting evidence provided by the visualization and analysis of individual chain motion, it becomes apparent that some type of knot formation and release is taking place albeit at discrete rather than universal times. We have been studying this phenomenon further to obtain the insight necessary to better understand the impact of knot formation and release on polymer entanglements.

In this study, we have performed discontinuous molecular dynamics simulations on a system of 32 hard

chain molecules of chain length 192 at each of three volume fractions, $\phi = 0.40, 0.45,$ and 0.50 . The quantities calculated over the course of the simulation include the mean squared displacement of the chain center of mass, the mean squared displacements of inner, outer, and intermediate segments along the chain, the end-to-end vector autocorrelation function, and the apparent diffusion coefficient. The relaxation behavior of these systems is compared to that predicted by the tube model and to that suggested for the release of interchain entanglements. To determine the extent to which our results exhibit tube confinement, we estimate the three relaxation times ($\tau_e, \tau_R,$ and τ_d) predicted by the tube model. The focus here is on determining whether the various methods for predicting the longest relaxation time, τ_d , yield results that are consistent with each other and with the simulation data. The longest relaxation time, τ_d , is predicted using three different tube model methods: (1) an estimate from the end-to-end vector autocorrelation function's relaxation behavior, (2) a calculation of τ_d from its defining equation, and (3) an estimate based on the predicted relationship between τ_d and τ_R . Next, we analyze the mean squared displacements of various groups of segments along the chain to determine both the progression of relaxation along the chain and the actual longest relaxation time without employing assumptions based on specific theories. Finally, the end-to-end vector autocorrelation function, outer segment mean squared displacement, and the apparent diffusion coefficient for each system are analyzed in light of a proposed mechanism of interchain entanglement relaxation which consists of three stages in time: initial relaxation, memory, and release.

Highlights from our simulation results are the following. During early times, the chain molecules' relaxation starts at the chain ends and progresses inward toward the chain middle as conjectured by the tube model. However, this trend does not persist throughout the relaxation, but instead reverses so that final relaxation occurs at the end segments instead of at the middle segments as predicted in the tube model. The tube model is not able to predict the mechanism of final relaxation nor is it able to predict the longest relaxation time, τ_d , consistently or accurately. This suggests that another method of entanglement release must be occurring during the simulations. The relaxation of specific interchain entanglements, or knots, like those described in the local knot theory^{5,6} and double reptation,⁷⁻¹⁰ might contribute to the observed dynamic behavior. A proposed mechanism of entanglement release, that of interchain entanglements or knots, is discussed in light of the simulation results. A simultaneous analysis of the results for the end-to-end vector autocorrelation function, the outer segment mean squared displacement, and the apparent diffusion coefficient supports the idea that knots are released through a mechanism of initial relaxation, followed by memory and final release. However, the uncertainty in these properties is large at the times when possible knot release behavior is exhibited; thus, caution is necessary when drawing conclusions from these results. Comparing the end-to-end vector autocorrelation function results from the systems at the three different packing fractions reveals that both the duration of knot constraints and the time of knot release increase as the packing fraction is increased.

The remainder of the paper is organized as follows. Section II describes the molecular model and simulation

techniques and presents the static properties of the chain systems. Section III provides relevant background information on chain dynamics and the tube model. Section IV describes our simulation results. A brief summary of our conclusions and some further discussion are given in section V.

II. Molecular Model and Simulation Methods

In this study, a polymeric fluid is modeled as a system of hard chains and simulated using the discontinuous molecular dynamics (DMD) technique used by Smith et al.³⁸ We begin this section by describing the molecular model for the chain molecules and reviewing the DMD technique as it is applied to this model. We then outline our method for constructing and relaxing the model polymer melts and present the static properties of the systems.

Because polymers are large molecules, their macroscopic behavior is dictated more by molecular size and geometry than by chemical structure. This suggests that the main features of polymers which must be incorporated into a model are the chain connectivity and the excluded volume of the segments. To model these features, Flory⁴¹ proposed the tangent hard sphere model which consists of hard spheres with bonds of fixed length equal to the segment diameter, σ . In this model, adjacent spheres are allowed to assume any bond angle that maintains tangency but prevents sphere overlap, thus allowing the model polymers to possess some degree of flexibility. However, the fixed bond constraint adds rotational velocities to the system and increases the complexity of the dynamics calculations, a drawback from the molecular dynamics point of view.

To circumvent this problem, Rapaport⁴² modified the tangent hard chain model to allow the bond length to vary by a fraction δ which is much smaller than the segment diameter σ . In effect, the segments, or beads, of the chain are joined by short strings of length $\delta\sigma$. To maintain the average bond length of the tangent hard chain model, Bellemans et al.⁴³ modified the Rapaport model to allow adjacent segments of a chain to interpenetrate by a distance equal to the length of the strings. With this modification, the bond length can vary over the range $(1 \pm \delta)\sigma$ with an average value approximately equal to the segment diameter, σ , as in the tangent hard sphere model. The added freedom of movement (in the Rapaport and Bellemans models) partially decouples the motion of the chain segments and greatly simplifies the calculation of segment trajectories.

All simulations in this study employed the hard chain model with Belleman's bonding constraints. The potential of interaction $U(r)$ between two nonbonded segments on the same or different chains is given by

$$U(r) = \begin{cases} \infty & r \leq \sigma \\ 0 & r > \sigma \end{cases} \quad (1)$$

where r is the distance between two segments and σ is the segment diameter. The potential energy between two bonded segments of a chain is given by

$$U(r) = \begin{cases} \infty & r \leq (1 - \delta)\sigma \\ 0 & (1 - \delta)\sigma < r < (1 + \delta)\sigma \\ \infty & r \geq (1 + \delta)\sigma \end{cases} \quad (2)$$

In this work, the bond extension parameter, δ , was set

to 0.1, since this provides sufficient displacement of the molecules while prohibiting chain crossing.

The simulations were performed using the discontinuous molecular dynamics technique used by Smith et al.³⁸ for hard chains. This method is essentially an extension of the DMD method developed by Alder and Wainwright⁴⁴⁻⁴⁶ for hard spheres to include bond stretch events. An event, or collision, occurs when the distance between two segments becomes equal to a discontinuity in the potential. Thus, the chains experience two possible types of collisions, core collisions (two segments coming into contact) and bond stretches (two bonded segments reaching their maximum separation distance). The DMD technique for simulating systems with discontinuous potentials takes advantage of the fact that linear trajectories between collisions produce equations of motion that can be solved analytically at successive collisions.

The simulations develop on a collision-by-collision basis by locating the next event in the system (core collision or bond extension), advancing the system to that point in time, computing the collision dynamics, and repeating the process. Possible events, core collisions and bond stretches, are investigated to determine the time when they will occur. A schedule of collision times is maintained to determine the sequence of events over the course of the simulation. Once the next event is determined, all the segments are advanced until that event occurs. The elastic event between two segments changes the magnitude and direction of their velocities. Since the velocities of the colliding particles change, their paths and thus their future collision partners will also change. Updating the collision lists requires the calculation of new collision times and partners for the colliding segments after each event; this is the most CPU intensive part of a discontinuous molecular dynamics simulation.

DMD has the inherent advantage that the trajectories of only a few particles change at each event; therefore, information must be updated for just a few particles instead of for the whole system. While this is an advantage when operating in series, it would not provide a worthwhile speed increase when operating in parallel. For this reason, the simulation of really huge systems (10^5 – 10^6 particles) using DMD methods would not be practical, but large systems may be simulated by employing efficiency techniques.

Because of the great computational demand associated with calculating new collision times, considerable effort has focused on improving the efficiency of this part of the simulation. The time needed to update the collision and partner lists is decreased by using a number of efficiency techniques as discussed in detail by Smith et al.,³⁸ including neighbor lists,⁴⁷ linked lists,⁴⁷ binary trees,⁴⁸ and false positioning.⁴⁹ The use of neighbor lists restricts the search for collision partners to a spherical volume with a specified radius around a given segment. Linked lists decrease the calculations needed to reconstruct the neighbor lists by restricting neighbor calculations to particles within adjacent subcells. Binary trees are used for efficient scheduling of the successive events to occur in the simulation, and false positioning is used to delay position updates to occur after a specified number of events instead of at every event. The use of these techniques has allowed us to simulate systems of long chain

Table 1. Size and Length of the Simulated Systems^a

n	N_c	ϕ	collisions $\times 10^{-9}$	$t^* \times 10^{-6}$
96	32	0.50	50	0.959
192	32	0.40	20	0.311
	32	0.45	82	1.03
	32	0.50	200	1.92
300	64	0.45	940	3.77
	64	0.50	1052	3.23

^a The sizes of the simulated systems are given in terms of the chain length, n , and the number of chains, N_c . Other simulation parameters include the packing fraction, ϕ , the number of collisions reported in billions of events, and the total reduced simulation time, t^* .

molecules over more than 6 orders of magnitude in reduced time.

Discontinuous molecular dynamics simulations were performed on systems containing 32 chains of length 192 at three different volume fractions, $\phi = 0.40, 0.45,$ and 0.50 . The volume fraction is the fraction of the system volume occupied by chain segments and is defined as $\phi = \pi N \sigma^3 / 6V$, where N is the total number of chain segments and V is the volume of the simulation cell. The simulations were performed in a cubic simulation cell with standard periodic boundary conditions.

Starting configurations at the three volume fractions studied were obtained by starting with a single initial configuration at a volume fraction of $\phi = 0.28$ and then increasing the volume fraction to the desired value. The initial configuration was generated by constructing each chain from a random walk with a bond length of $(1 + \delta/2)\sigma$ and assigning random velocities to each segment using a Gaussian number generator. After the initial configuration was obtained, the velocities were scaled to obtain an average segment velocity of $v = 0$ and a reduced system temperature of $k_B T = 1.0$. The volume fraction of the system was then increased by growing segment diameters at bond stretch events³⁸ while performing the discontinuous molecular dynamics simulation with the nonoverlapping Rapaport model mentioned above. The starting configurations at $\phi = 0.40, 0.45,$ and 0.50 were obtained when the volume fractions of interest were reached. Each of these three starting configurations was then relaxed using the Bellemans model during the equilibration phase. Once the chain center of mass moved at least one radius of gyration, the equilibration phase was finished, and the production phase was started. A single long run was performed at each of the three volume fractions.

Table 1 summarizes the systems studied and includes the chain length, n , the number of chains, N_c , the volume fraction, ϕ , the number of collisions, and the total times sampled during the production phases of the simulations. The simulation times are presented throughout the paper in terms of reduced units, $t^* = ((k_B T / m \sigma^2))^{1/2} t$, where k_B is the Boltzmann constant, T is the temperature, and m is the mass of a segment. All simulations were performed at a reduced temperature of $k_B T = 1.0$ and a mass of $m = 1.0$ for all segments.

The static properties of the systems studied, including the mean squared end-to-end distance, $\langle R^2 \rangle$, the mean squared radius of gyration, $\langle R_G^2 \rangle$, and the compressibility factor, Z , were monitored over the course of the simulations to confirm fluid equilibration.

The mean squared end-to-end distance was calculated from

$$\langle R^2 \rangle \equiv \langle (\mathbf{r}_1 - \mathbf{r}_n)^2 \rangle \quad (3)$$

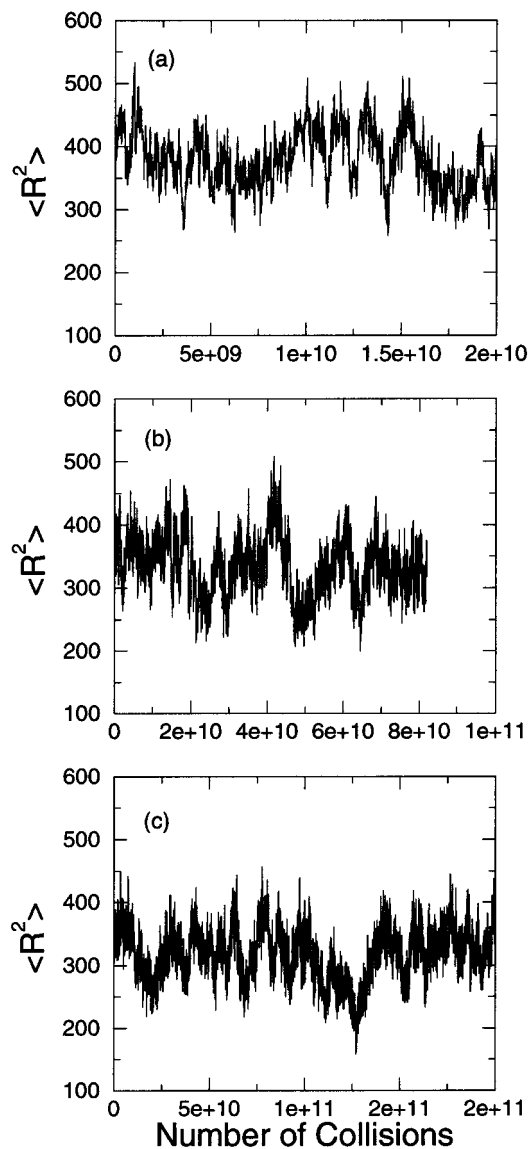


Figure 1. Mean squared end-to-end distance vs the number of collisions for chains of length 192 at (a) $\phi = 0.40$, (b) $\phi = 0.45$, and (c) $\phi = 0.50$.

where \mathbf{r}_1 and \mathbf{r}_n are the coordinates of the first and last chain segments and $\langle \rangle$ denotes an ensemble average. Figure 1 displays the system average mean squared end-to-end distance as a function of the number of collisions for chains of length 192 at (a) $\phi = 0.40$, (b) $\phi = 0.45$, and (c) $\phi = 0.50$. In a melt, excluded volume effects are screened so that the chains behave ideally and follow Gaussian statistics.⁴¹ For a Gaussian chain, the mean squared end-to-end distance follows the relationship:

$$\langle R^2 \rangle = l^2 l_p^2 (n - 1) \quad (4)$$

where l is the bond length, and l_p is the persistence length, which is a measure of chain stiffness. The average bond length decreases with increasing volume fraction as the system becomes more densely packed so that $l \approx 1.00, 0.99,$ and 0.98 at $\phi = 0.40, 0.45,$ and 0.50 . Linear regression analysis was performed using the mean squared end-to-end distance from this work listed in Table 2 along with that for chains of length $n = 8$ to $n = 192$ at $\phi = 0.40$ and 0.45 from Smith et al.¹¹ The persistence lengths for the three volume fractions

Table 2. Static Properties of the Systems^a

n	ϕ	$\langle R^2 \rangle$	$\langle R_g^2 \rangle$	$\langle R^2 \rangle / \langle R_g^2 \rangle$	Z
96	0.50	155.28(10.44)	25.65(1.30)	6.05	834.77(0.10)
192	0.40	379.68(28.13)	61.72(2.70)	6.15	761.71(0.14)
	0.45	331.69(36.08)	55.36(3.98)	5.99	1127.80(0.18)
300	0.50	317.44(35.23)	52.07(4.49)	6.10	1665.06(0.23)
	0.45	510.81(49.21)	85.47(5.50)	5.98	1760.01(0.26)
	0.50	485.26(38.72)	81.29(3.77)	5.96	2599.00(0.26)

^a The mean squared end-to-end distance, $\langle R^2 \rangle$, mean squared radius of gyration, $\langle R_g^2 \rangle$, the ratio of the sizes, $\langle R^2 \rangle / \langle R_g^2 \rangle$, and the compressibility factor, Z , are reported. The chain sizes are reported in units of σ^2 . Values in parentheses are the standard deviations.

studied are $I_p \approx 1.39, 1.32$, and 1.30 for $\phi = 0.40, 0.45$, and 0.50 , which decrease with increasing volume fraction, as expected.

The radius of gyration, another measure of chain size, describes the distribution of mass within the chain by

$$\langle R_g^2 \rangle \equiv \frac{1}{n} \left\langle \sum_{i=1}^n (\mathbf{r}_i - \mathbf{r}_{c.m.})^2 \right\rangle \quad (5)$$

where \mathbf{r}_i is the position of segment i and $\mathbf{r}_{c.m.} = 1/n \sum_{i=1}^n \mathbf{r}_i$ is the position of the chain center of mass. For a Gaussian chain, the radius of gyration should also scale linearly with chain length so that the ratio $\langle R^2 \rangle / \langle R_g^2 \rangle \approx 6$.⁴¹

The compressibility factor was calculated from the Clausius virial theorem in the following form

$$Z = n - \frac{m \sum_{\text{coll}} \mathbf{r}_{ij} \cdot \Delta \mathbf{v}_{ij}}{3N_c k_B T t_e} \quad (6)$$

where \mathbf{r}_{ij} is the vector between segment centers at a collision, $\Delta \mathbf{v}_{ij}$ is the velocity change for the colliding pair, N_c is the number of chains in the system, and t_e is the elapsed simulation time over which the sum is calculated.

The results for the static properties, $\langle R^2 \rangle$, $\langle R_g^2 \rangle$, $\langle R^2 \rangle / \langle R_g^2 \rangle$, and Z are presented in Table 2. The values obtained for $\langle R^2 \rangle / \langle R_g^2 \rangle$ indicate that the chains used in this study are essentially Gaussian. The compressibility factor was found to be linear with chain length and consistent with the work of Zhou et al.⁵⁰

Agreement between the static properties of the simulations and predicted behavior confirms the equilibration of the systems. With the confirmation of fluid equilibration, the production phases of the simulations were started in order to study the dynamic properties of the systems. A single long run was performed at each of the three volume fractions. During the course of the simulations, the coordinates of all chain segments were stored so that they could be used to determine the dynamic properties. Time correlation functions were calculated from the trajectories by averaging over different time origins using standard methods. The first 85% of the time steps were used as time origins in the dynamics analysis to increase the statistics of the results at the longer times. The dynamic properties which were studied are discussed in the next section.

III. Background on Chain Dynamics

In this section, we briefly review those aspects of chain dynamics and tube model predictions that are relevant to the discussion of the results. We begin by defining the mean squared displacement and the four scaling regimes postulated by the tube model.²⁷ We next

review the connection between the mean squared displacement and the self-diffusion coefficient. Finally, we define the end-to-end vector autocorrelation function and describe its relationship to the longest relaxation time in the tube model, τ_d .

Microscopic information about polymer diffusion is obtained by analyzing the time dependence of chain and chain-segment displacements. The atomic mean-squared displacement, $g(t)$, is the average squared distance a chain segment moves after a time, t , and is defined as

$$g(t) \equiv \frac{1}{n} \sum_{i=1}^n \langle |\mathbf{r}_i(t + t_0) - \mathbf{r}_i(t_0)|^2 \rangle \quad (7)$$

where $\mathbf{r}_i(t)$ is the position of atom i at time t , the sum is over all chain segments i , and $\langle \rangle$ represents the ensemble average which is over all time origins t_0 as well as over all molecules. As described in the Introduction, the tube model predicts that entangled polymer chains sample four time regimes of $g(t)$ scaling behavior: (1) $g \sim t^{1/2}$ for $t \leq \tau_e$, (2) $g \sim t^{1/4}$ for $\tau_e < t < \tau_R$, (3) $g \sim t^{1/2}$ for $\tau_R < t < \tau_d$, and (4) $g \sim t$ for $t > \tau_d$.²⁷

Analysis of the atomic mean squared displacement is often restricted to the inner segments of the chain to distinguish between effects of high mobility of segments near the chain ends and low mobility of segments near the chain middle. The mean squared displacement averaged over k segments in the chain middle is calculated from

$$g_{\text{in}}(t) \equiv \frac{1}{k} \sum_{i=n/2+1-k/2}^{n/2+k/2} \langle |\mathbf{r}_i(t + t_0) - \mathbf{r}_i(t_0)|^2 \rangle \quad (8)$$

During this study, we restricted the inner segment mean squared displacement to the 10 segments in the chain middle.

The macroscopic self-diffusion coefficient, D , is obtained from the long-time mean squared displacement of the chains, according to

$$D = \lim_{t \rightarrow \infty} \frac{g_{\text{cm}}(t)}{6t} \quad (9)$$

where $g_{\text{cm}}(t)$ is the center of mass mean squared displacement. The center of mass mean squared displacement is defined as

$$g_{\text{cm}}(t) \equiv \frac{1}{N_c} \sum_{i=1}^{N_c} \langle |\mathbf{r}_{i,\text{cm}}(t + t_0) - \mathbf{r}_{i,\text{cm}}(t_0)|^2 \rangle \quad (10)$$

where $\mathbf{r}_{i,\text{cm}}(t)$ is the position of the center of mass of chain i at time t , the sum is over all chains i and $\langle \rangle$ represents the ensemble average which is over all time origins t_0 as well as over all molecules. Throughout the paper, the mean squared displacements are reported in reduced units by dividing by the diameter squared, σ^2 .

Information about stress relaxation, and hence viscosity, is obtained from the end-to-end vector autocorrelation function.²⁷ The end-to-end vector autocorrelation function is defined by

$$C_R(t) \equiv \langle \mathbf{R}(t + t_0) \cdot \mathbf{R}(t_0) \rangle / \langle R^2 \rangle \quad (11)$$

where $\mathbf{R}(t)$ is the vector between the chain ends at time t , $\langle R^2 \rangle$ is the mean squared end-to-end distance of the chains in the system, and the averages are taken over

all chains and over all time origins, t_0 . The end-to-end vector autocorrelation function provides a measure of the relaxation of chain orientation by monitoring how much the vectors between the chain ends remain correlated over time.

In the tube model, the end-to-end vector autocorrelation function is a measure of the average fraction of the chain remaining in the original tube, or equivalently the fraction of the original tube remaining after a time t .²⁷ The tube model assumes each chain moves solely along its own contour by reptation with a curvilinear diffusion constant, D_c . Since chain ends are able to leave the tube, once a chain end reaches a tube section, that portion of the tube vanishes. On the basis of these assumptions, Doi and Edwards²⁷ derived an equation for the fraction of the tube remaining at time t

$$\psi(t) = \sum_{p:\text{odd}} \frac{8}{p^2 \pi^2} \exp(-p^2 t / \tau_d) \quad (12)$$

where

$$\tau_d = \frac{L^2}{D_c \pi^2} \quad (13)$$

L is the contour length of the primitive chain, and D_c is the curvilinear diffusion coefficient. Because the end-to-end vector autocorrelation function, $C_R(t)$, measures the portion of the end-to-end vector which remains correlated after time, t , it should be equivalent to the fraction of the tube remaining, ψ , i.e.²⁷

$$\psi(t) \approx C_R(t) \quad (14)$$

for $t \geq \tau_e$. This provides a relationship between the end-to-end vector autocorrelation function, $C_R(t)$, and the longest relaxation time, τ_d , and allows τ_d to be estimated by fitting the measured $C_R(t)$ data to the following equation:

$$C_R(t) \approx \sum_{p:\text{odd}} \frac{8}{p^2 \pi^2} \exp(-p^2 t / \tau_d) \quad (15)$$

IV. Results and Discussion

In this section, we present and discuss the results from our molecular dynamics simulations. The section is divided into three subsections. In the first subsection, we use our simulation results to estimate the three relaxation times of the tube model, τ_e , τ_R , and τ_d . Three different methods, all prescribed by the tube model, are used to predict the final relaxation time, τ_d . The idea here is to determine whether the various methods for predicting τ_d yield results that are consistent with each other and with the simulation data. In the second subsection, we analyze the mean squared displacements of the chain center of mass and chain segments at various positions along the chain. This analysis is used to determine the progression of relaxation along the chains and to identify the final relaxation time of each system without making assumptions based on any particular theory. In the third subsection, we analyze the end-to-end vector autocorrelation function, the outer segment mean squared displacement, and the apparent diffusion coefficient to show the agreement of our simulation results with a proposed mechanism for interchain entanglement release consisting of three

Table 3. Estimated Tube Model Relaxation Times^a

n	ϕ	τ_e	τ_R	$\tau_d(C_R)$	$\tau_d(D)$	$\tau_d(\tau_R)$
192	0.40	1800	25 000	53 000	80 240	360 000
	0.45	3000	67 000	101 000	149 000	965 000
	0.50	4500	100 000	240 000	312 700	1 440 000

^a The entanglement time, τ_e , the Rouse time, τ_R , the longest relaxation time as estimated from the end-to-end vector autocorrelation function, $\tau_d(C_R)$, the longest relaxation time as calculated from the defining equation, $\tau_d(D)$, and the longest relaxation time, $\tau_d(\tau_R)$, as estimated from the predicted ratio between τ_R and τ_d .

stages in time, initial relaxation, memory, and release from a chain end.

A. Tube Model Entanglement Relaxation and Release. In the tube model, chain molecules experience three different relaxation times which mark changes in the mean squared displacement power law scaling with time as a result of entanglements.²⁷ The first relaxation time, τ_e , is referred to as the entanglement time, because it marks the onset of entanglement constraints. The second relaxation time, τ_R , indicates the beginning of entanglement relaxation and marks the time when the chain ends begin to diffuse out of the tube. During this regime, relaxation of the tube constraints progresses from the chain ends toward the chain middle until final relaxation is achieved at τ_d . The final relaxation time, τ_d , is the time after which the chains experience free diffusion. Studying relaxation in the time regime between τ_R and τ_d is the key to determining whether the release of entanglements follows the physical description given in the tube model.

Table 3 displays the relaxation time estimates for τ_e , τ_R , and τ_d obtained for chains of length 192 at $\phi = 0.40$, 0.45, and 0.50. Three different τ_d estimates, which we will call $\tau_d(C_R)$, $\tau_d(D)$, and $\tau_d(\tau_R)$, are obtained using three different tube model methods. The methods used to obtain these relaxation times are described below.

Entanglements, in the form of tube confinement, begin to hinder the lateral motion of chain molecules at the first relaxation time, τ_e .²⁷ At this time, the chain segments have moved a distance on the order of the tube diameter and, thus, begin to feel the lateral constraints of the confining tube. This will cause the mean squared displacement scaling exponent to decrease.

The entanglement time, τ_e , of each system was estimated by determining the time at which the inner segment mean squared displacement vs time experienced a decrease in slope on a log-log plot. For the 192mer systems, these times, in reduced units, are $\tau_e \approx 1800$, 3000, and 4500 at volume fractions $\phi = 0.40$, 0.45, and 0.50, respectively. Increasing volume fraction produces two competing effects on τ_e . The distance the chains must move in order to experience tube confinement decreases as volume fraction increases since the tube diameter decreases with increasing volume fraction; this effect tends to decrease τ_e . However, the mobility of the chains and their segments decreases as the volume fraction increases, and this tends to increase τ_e . We find that the value of τ_e increases with increasing volume fraction indicating that the decrease in chain mobility as the system becomes more densely packed is the dominant effect.

The Rouse time, τ_R , designates the beginning of tube decay and thus entanglement relaxation.²⁷ At τ_R , the chain begins to diffuse up and down the tube allowing its ends to leave the tube. This causes the tube to begin decaying from the ends toward the middle, since segments near the tube ends are able to escape their

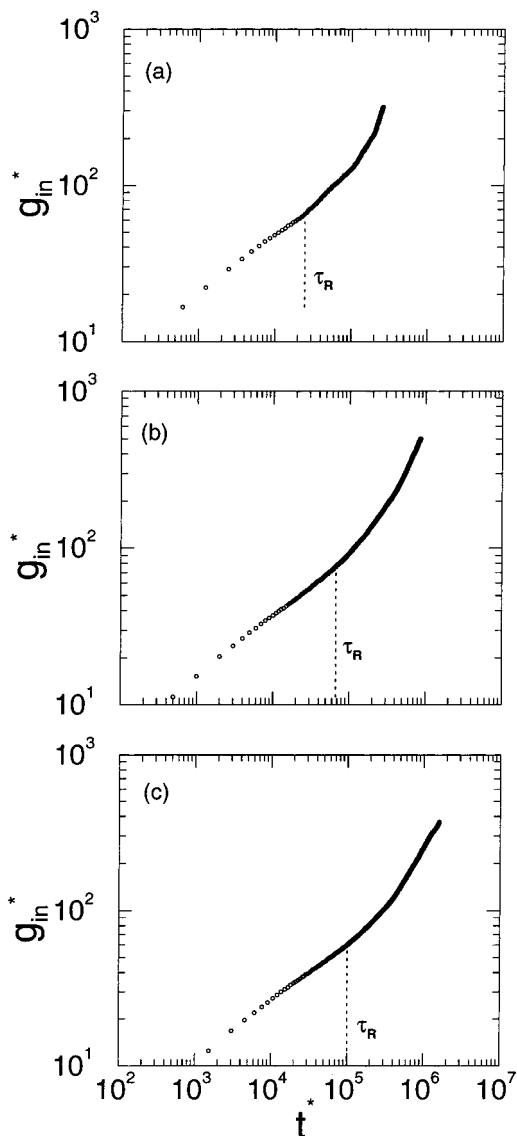


Figure 2. Inner segment mean squared displacement vs reduced time for chains of length 192 at (a) $\phi = 0.40$, (b) $\phi = 0.45$, and (c) $\phi = 0.50$. The dashed lines represent the relaxation time, τ_R , as listed in Table 3.

confinement. As the confinement decreases at τ_R , the segment mobility begins to increase, causing the mean squared displacement power law exponent to increase.

The Rouse time, τ_R , was estimated as the time at which the inner segment mean squared displacement experiences an increase in slope when plotted on a log–log scale. Figure 2 is a log–log plot of the inner segment mean squared displacement for the 192mer fluid vs reduced time which shows the τ_R estimates, $\tau_R \approx 25\,000$, $67\,000$, and $100\,000$, at (a) $\phi = 0.40$, (b) $\phi = 0.45$, and (c) $\phi = 0.50$, as listed in Table 3. Like the value of τ_e , the value of τ_R also increases with increasing packing fraction, indicating that the decrease in chain mobility which occurs with increased density also delays the time at which entanglement relaxation begins.

Investigating the mean squared displacement behavior in the regime between τ_R and τ_d helps to determine if the release of entanglements follows the physical description given by the tube model. This is the time period when entanglement relaxation and release is an important factor in chain dynamic behavior. According to the tube model, entanglements begin to relax, at τ_R ,

from the chain ends toward the chain middle as more segments escape the tube. This relaxation should continue until complete relaxation occurs at τ_d , the longest relaxation time of the system. The estimates for τ_R and τ_d pinpoint the appropriate time range for investigating the behavior of entanglement release.

The tube model provides a number of different methods for estimating τ_d .²⁷ The first method for estimating τ_d is to determine the time it takes for the end-to-end vector autocorrelation function to relax to $C_R(\tau_d) \approx 0.2982$, as given by eq 15 of the tube model for the fraction of tube remaining. The second method for estimating τ_d is to use the definition for τ_d , given in eq 13, which describes τ_d as the time it takes a chain to diffuse the length of its tube. The third method for estimating τ_d is provided by the predicted relationship between τ_d and τ_R . If the tube model is a good representation of the data, the estimates from these three different methods should be equivalent.

The first method used to estimate τ_d is to determine the time at which the end-to-end vector autocorrelation function data has relaxed sufficiently as described by eq 15 derived from the tube model. The end-to-end vector autocorrelation function, $C_R(t)$, is calculated from the data using eq 11. Since τ_d is the only parameter in eq 15 for $C_R(t)$, it can be estimated from the time at which $C_R(\tau_d) \approx \psi(\tau_d) \approx 0.2982$. We designate the relaxation time found from this method as $\tau_d(C_R)$. Using this method for the 192mer systems, yields the following estimates: $\tau_d(C_R) \approx 53\,000$, $101\,000$, and $240\,000$ at $\phi = 0.40$, 0.45 , and 0.50 . As was the case for our estimates for τ_e and τ_R , this relaxation time increases with increasing ϕ , indicating that it takes longer for the more dense, and thus more entangled, systems to relax.

Figure 3 displays the end-to-end vector autocorrelation functions, $C_R(t)$, calculated directly from the 192mer data at (a) $\phi = 0.40$, (b) $\phi = 0.45$, and (c) $\phi = 0.50$ using eq 11. The tube model predictions for $C_R(t)$, eq 15, using the τ_d values above, are also included in the figure. At times up to and just beyond $\tau_d(C_R)$, the theory fits the C_R data well; however, the exponential equation is a poor representation of the data at later times.

In the second method, τ_d is calculated from its definition, eq 13, which estimates the time it takes a chain to diffuse the length of its confining tube. Since eq 13 is in terms of curvilinear tube coordinates, it must be converted to the laboratory reference frame for calculation.²⁷ This yields

$$\tau_d = \frac{\langle R^2 \rangle}{3\pi^2 D} \quad (16)$$

where D is the self-diffusion coefficient in the laboratory reference frame.

Using eq 16 to calculate τ_d , designated $\tau_d(D)$, requires an estimate for D . The self-diffusion coefficient, D , is the long-time asymptotic value of the apparent self-diffusion coefficient, $D_{app}(t)$ which is related to the center-of-mass mean squared displacement according to the following relationship:

$$D_{app}(t) \equiv \frac{\langle [\mathbf{r}(t) - \mathbf{r}(0)]^2 \rangle}{6t} \equiv \frac{g_{cm}(t)}{6t} \quad (17)$$

During the early time regimes, $t < \tau_R$, the chain center of mass is predicted to experience anomalous diffusive

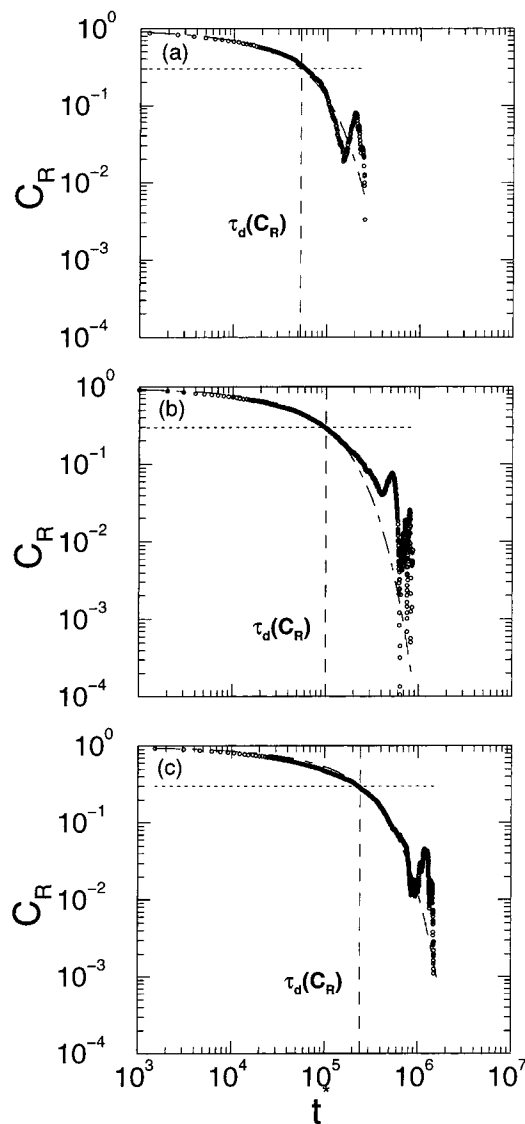


Figure 3. End-to-end vector autocorrelation function vs reduced time for chains of length 192 at (a) $\phi = 0.40$, (b) $\phi = 0.45$, and (c) $\phi = 0.50$. The circles represent the simulation results, the dotted lines represent $C_R(\tau_d) \approx 0.2982$, the dashed lines represent the estimated values for $\tau_d(C_R)$, and the dot-dashed lines represent the tube model predictions for $C_R(t^*)$.

behavior where the mean squared displacement scaling behavior and thus $D_{app}(t)$, vary with time. The long time limit of $D_{app}(t)$ is the self-diffusion coefficient, D , as given by the following Einstein relation:^{51,52}

$$D = \lim_{t \rightarrow \infty} \frac{\langle [\mathbf{r}(t) - \mathbf{r}(0)]^2 \rangle}{6t} \quad (18)$$

Figure 4 shows $D_{app}(t)$ vs t^* on a log-log plot for the 192mer fluids at (a) $\phi = 0.40$, (b) $\phi = 0.45$, and (c) $\phi = 0.50$. According to the tube model, the quantity $D_{app}(t)$ should decrease with time until it reaches a long-time plateau at the value D . However, a long-time plateau was not observed in our simulations; therefore, the diffusion coefficient was estimated instead from the minimum value of $D_{app}(t)$, because this provides the longest possible time for $\tau_d(D)$ as calculated from eq 16. Using this method, the estimates obtained for the self-diffusion coefficient, in reduced units, are $D^* \approx 1.47 \times 10^{-4}$, 7.73×10^{-5} , and 3.51×10^{-5} at $\phi = 0.40$, 0.45 ,

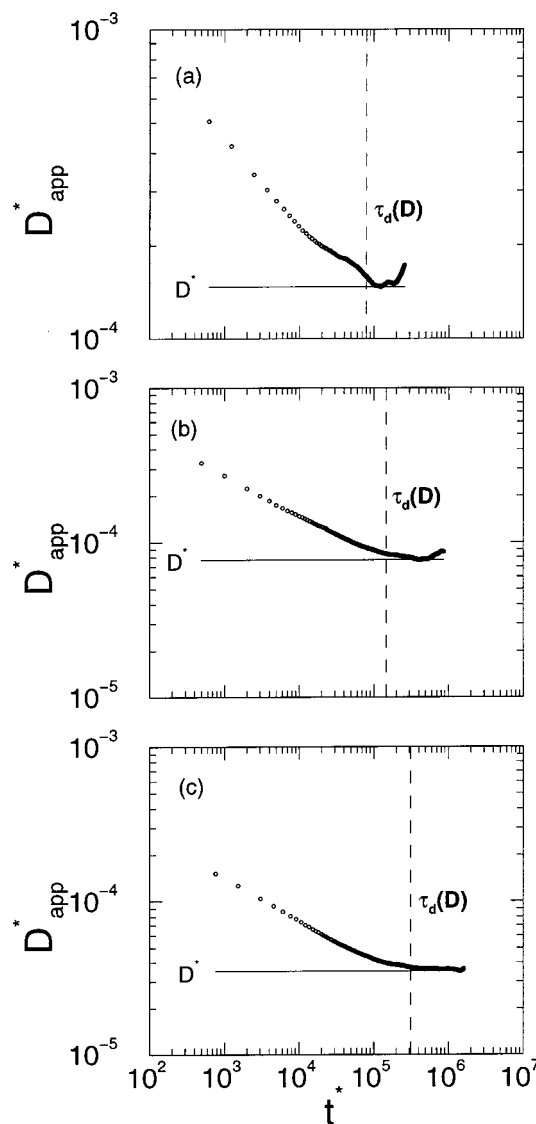


Figure 4. Apparent self-diffusion coefficient vs reduced time for chains of length 192 at (a) $\phi = 0.40$, (b) $\phi = 0.45$, and (c) $\phi = 0.50$. The circles represent the simulation results, the horizontal lines represent the estimated self-diffusion coefficient, and the dashed lines represent the calculated values for $\tau_d(D)$.

and 0.50. From these estimates, the longest relaxation times for the 192mers were calculated from eq 16 to be $\tau_d(D) \approx 80\,240$, $149\,000$, and $312\,700$ for $\phi = 0.40$, 0.45 , and 0.50 . Each of these estimates is larger than the corresponding $\tau_d(C_R)$ estimate obtained from the $C_R(t)$ data; however, these two methods give results that are of the same order of magnitude.

The third method used to estimate τ_d is based on the following relationship between τ_d and τ_R provided by the tube model²⁷

$$\tau_d = 3z\tau_R \quad (19)$$

where $z = N/N_e$ with N_e equal to the entanglement length for the system. The entanglement length is the largest subchain which does not feel entanglement constraints. It can be estimated by relating the tube diameter, d_T , estimated from the mean squared displacement at τ_e , to the end-to-end distance of a chain of length N_e through $g(\tau_e) \approx d_T^2 = \langle R^2(N_e) \rangle / 3$ leading to^{22,24}

$$N_e \approx \frac{3g(\tau_e)}{(ll_p)^2} + 1 \quad (20)$$

where we use the inner segment mean squared displacement for g . Using this method, we obtained the estimates $N_e \approx 40, 43,$ and 37 at $\phi = 0.40, 0.45,$ and 0.50 . The error in these estimates is greater than the difference between them; therefore, we used the average value of $N_e \approx 40$ for all of the systems. Our estimate of $N_e \approx 40$ is similar to that obtained from other comparable studies. In previous literature, values of $28 < N_e < 38$ were obtained using comparable methods.^{11,19,21,22,24} Kremer and Grest²² reported $N_e \approx 35$, Paul et al.¹⁹ reported $N_e \approx 30$, Smith et al.¹¹ reported $29 < N_e < 35$, Pütz et al.²⁴ reported $28 < N_e < 35$, and Kreer et al.²¹ reported $35 < N_e < 38$. However, the question remains as to whether the mean squared displacement results provide the correct value of N_e . For example, when using the plateau modulus to estimate N_e , Pütz et al.²⁴ obtained $65 < N_e < 83$ or about 2.3 times the estimate obtained from the mean squared displacement.

The values of τ_R listed in Table 3 were used along with our entanglement length estimate of $N_e \approx 40$ at all volume fractions to obtain a third estimate for τ_d , which we will call $\tau_d(\tau_R)$, from eq 19. From this method we find that $\tau_d(\tau_R) \approx 360\,000, 965\,000,$ and $1\,440\,000$ at $\phi = 0.40, 0.45,$ and 0.50 , respectively. These values are significantly larger than both $\tau_d(C_R)$ and $\tau_d(D)$ obtained above.

The three tube model methods for estimating τ_d provide vastly different values for $\tau_d(C_R), \tau_d(D),$ and $\tau_d(\tau_R)$, and hence provide inconsistent predictions for the longest relaxation time, τ_d . This suggests that either the tube model is not accurate in its simplest form or the systems studied here are not sufficiently entangled to be represented by the theory.

B. Actual Relaxation of the Mean Squared Displacement Results. The lack of agreement between the three different methods for estimating τ_d prescribed by the tube model prompted us to analyze the mean squared displacement behavior during the relaxation time range in more depth, with particular focus on both the progression of relaxation along the chain and the actual final relaxation time of each system. By analyzing the mean squared displacements of segments at different positions along the chain, we are able to determine how segment position affects the time when entanglement relaxation occurs and hence obtain information about the mechanism of entanglement relaxation and release. As mentioned above, the tube model dictates that tube relaxation starts at the chain ends and progresses along the chain toward the chain middle where final relaxation occurs. In contrast, interchain entanglements will only be released when a chain end passes through the knot. We can also use the different mean squared displacements to estimate the final relaxation time without resorting to assumptions based on specific theories. This is possible because final relaxation results in free diffusion of the chains and chain segments causing all of the mean squared displacements to exhibit the same power law exponent of 1.

We analyzed the mean squared displacements of the following groups of segments: the center of mass, the 10 inner segments in the chain middle, intermediate segments along the chain, and the five outer segments at each chain end. The intermediate segments whose motion was analyzed include the following groups of 10

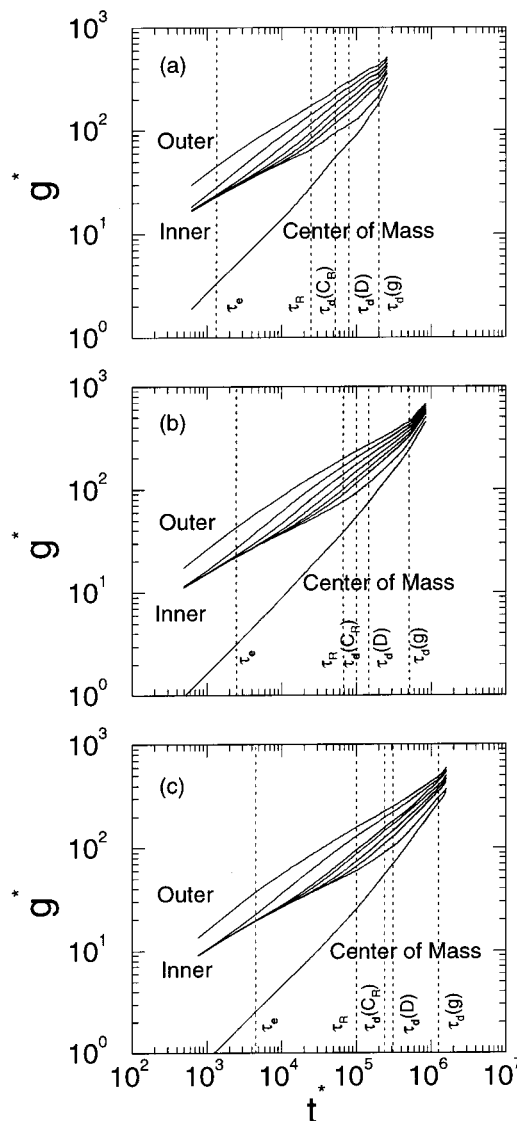


Figure 5. Mean squared displacement vs reduced time for chains of length 192 at (a) $\phi = 0.40$, (b) $\phi = 0.45$, and (c) $\phi = 0.50$. The top curve is for the 5 outer segments at each chain end. The next five curves are for blocks of segments at intermediate positions along the chain. The second curve from the bottom is for the 10 inner segments in the chain middle, and the bottom curve is for the chain center of mass. The dashed lines mark the estimated relaxation times, $\tau_e, \tau_R, \tau_d(C_R), \tau_d(D),$ and $\tau_d(g)$.

segments (five from each side of the chain): segments 11–15 and 178–182, segments 21–25 and 168–172, segments 31–35 and 158–162, segments 41–45 and 148–152, and segments 51–55 and 138–142. Figure 5 displays the various mean squared displacements as a function of reduced time for the 192mer systems at (a) $\phi = 0.40$, (b) $\phi = 0.45$, and (c) $\phi = 0.50$. In the figure, dashed lines mark the estimated relaxation times, $\tau_e, \tau_R, \tau_d(C_R), \tau_d(D),$ and $\tau_d(g)$ (defined below). The times sampled show a range of mean squared displacement behavior as discussed below.

At the early times ($t^* < \tau_e$) shown in Figure 5, segment motion is dominated by small-scale fluctuations of segment positions, which do not result in much overall chain displacement. During this time regime, the center-of-mass mean squared displacement is an order of magnitude smaller than that of the chain segments, indicating that the segmental motion is mainly a result of small-scale fluctuations of segment positions which

do not produce much overall displacement of the chain center of mass. Comparing the early-time mean squared displacements of the various segments along the chain provides information about these fluctuations and how they relate to entanglement relaxation. At the earliest times shown in Figure 5, all of the segments, except the outermost segments (top curve), have moved approximately the same distance. This indicates that chain connectivity is the dominant factor during this time range, as the tube model dictates. The end segments are able to move more than the other segments because they are bound on only one side while the other segments are bound on both sides.

As time increases, the various mean squared displacements begin to fan out as intermediate segments near the chain ends experience more relaxation than the inner segments causing the slopes of their mean squared displacement curves to increase. First, the chain sections which include segments 11–15 and 178–182 (second curve from top) begin to relax which causes their mean squared displacement slope to increase. Then, this relaxation progresses to the next section (segments 21–25 and 168–172) along the chain closer to the chain middle and continues with the next sections in order toward the chain middle. This indicates that the initial relaxation of entanglements occurs near the chain ends and progresses toward the chain middle with time. The tube model predicts this type of behavior; however, it is expected to occur later, during the time range between τ_R and τ_d , as an increasing number of segments escape the original confining tube. In our system, this behavior begins to occur at approximately τ_e but may be a result of analyzing segments that are still too close to the chain ends to experience tube confinement.

Although the initial entanglement relaxation follows the tube model prediction that relaxation begins with the outer segments and moves inward toward the inner segments, this trend does not continue until the final relaxation of entanglements. At times between τ_R and τ_d , the slopes of the inner segment mean squared displacement curves increase, as predicted by the tube model. At the same time, the slopes of the outer segment mean squared displacement curves decrease slightly. To achieve free diffusion (the time regime that occurs for $t^* > \tau_d$), the outer segment mean squared displacement curves in Figure 5 switch from concave down to concave up. In contrast, the inner segment mean squared displacement curves continue to undergo a smooth increase toward free diffusion. The outer segment mean squared displacement slope increases more than that of the inner segments, indicating that a considerable amount of relaxation occurs near the end segments before free diffusion is reached. This is in contrast to the tube model idea which says that final relaxation of the tube occurs in the chain middle, but is in agreement with the idea of interchain entanglements which must be released from a chain end.

Once a system has achieved complete relaxation, as is expected to occur after the longest relaxation time, τ_d , the chains and all of their segments should diffuse freely. Beyond τ_d , the mean squared displacements for all segments along the chain should display uniform scaling behavior with slopes equal to 1 on a log–log plot of g^* vs t^* .

To determine if and when this occurs, we compare the mean squared displacement behavior of the chain center of mass to that of the various segments along the chain.

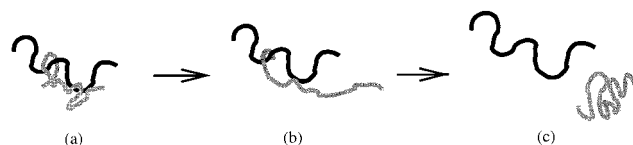


Figure 6. Proposed mechanism for knot disentanglement and release showing (a) initial relaxation, (b) chain stretching before release from chain end, and (c) large displacement and relaxation achieved following knot release.

We find that a transition toward uniform mean squared displacement scaling behavior occurs at approximately $t^* \approx 202\,000$, $579\,000$, and $1\,275\,000$ for $\phi = 0.40$, 0.45 , and 0.50 . These times are designated $\tau_d(g)$ and are indicated by dashed lines in Figure 5. As was the case with all of the relaxation time estimates, $\tau_d(g)$ increases with increasing packing fraction.

The transition to similar mean squared displacement scaling behavior, $\tau_d(g)$, occurs at a later time than both $\tau_d(C_R)$ and $\tau_d(D)$. Since our estimate of $\tau_d(g)$ is not based on any particular theory, but is instead based on a comparison of the mean squared displacements of the chain center of mass and the mean squared displacements of various segments at different positions along the chain, it provides a more accurate estimate of τ_d than the methods used in the previous subsection. Because additional relaxation is occurring at $\tau_d(g)$, the actual longest relaxation time of the system cannot be any earlier than $\tau_d(g)$. This indicates that the estimated values $\tau_d(C_R)$ and $\tau_d(D)$ are too low and do not correspond to the actual final relaxation times for the systems studied. However, the estimated values $\tau_d(\tau_R)$ are longer than $\tau_d(g)$ and the longest times analyzed.

The addition of modifications to the tube model, including contour length fluctuations^{53–56} and constraint release,^{57–60} would add other modes of entanglement release. However, constraint release would not affect τ_d significantly, and contour length fluctuations would decrease τ_d , thus increasing the discrepancy between the tube model predictions and the actual relaxation of the mean squared displacements. To obtain closer agreement with our simulation results, the tube model would need to be modified to include additional entanglement constraints instead of additional relaxation methods. This suggests that another form of entanglements is present in our systems.

C. Interchain Entanglement Release. Entanglement relaxation as proposed by the tube model does not sufficiently describe the release of the entanglements in the systems studied here; therefore, another method of entanglement release, possibly that of interchain entanglements, or knots, like those described in the local knot theory^{5,6} and double reptation,^{7–10} must also be occurring in these systems. The mechanism of interchain entanglement release is quite different than the relaxation of a chain confined to a tube. Interchain entanglements are released only when a chain end is able to pass through the entanglement or knot; therefore, this type of entanglement release will occur at a chain end. In this subsection, we describe evidence that entanglement release consistent with the release of interchain entanglements, or knots, is occurring in the systems studied.

Our simulation results suggest that interchain entanglement relaxation progresses through three stages; initial relaxation, memory, and release, as illustrated schematically in Figure 6. First a knotted chain experiences some relaxation. Second the constraints from the

knot start to have an impact, hindering the chain's relaxation by pulling part of it back toward its previous position which provides the chain with a memory of its previous orientation. During this stage, the chain stretches since the knotted chain portion is restricted to its previous conformation while the unconstrained portions continue to relax. Finally a chain end passes through the knot and releases the entanglement. The chain then moves quickly to release the energy stored during the previous stretching so as to obtain a more favorable conformation. The mechanism of interchain entanglement release proposed here is supported by the behavior described below.

A combined analysis of the end-to-end vector autocorrelation function, the outer segment mean squared displacement, and the apparent diffusion coefficient provides support for the proposed mechanism of interchain entanglement release. The behavior of (a) the end-to-end vector autocorrelation function, (b) the outer segment mean squared displacement, and (c) the apparent self-diffusion coefficient is presented for the 192mer systems at $\phi = 0.40, 0.45,$ and 0.50 in Figures 7–9, respectively. The dashed lines in the figures bound the time range when knot constraints appear to affect the systems. All of the systems display similar behavior. The combined analysis of these three quantities paints a compelling picture of the proposed mechanism of entanglement release.

The results for the end-to-end vector autocorrelation function (in Figures 7a, 8a, and 9a) illustrate the complicated relaxation of chain orientation, which includes initial relaxation, memory (stretching), and release. First, an initial relaxation of the chains is observed as the autocorrelation function decreases. This is followed by an increase in the autocorrelation function, and thus chain orientation, when the knot constraints take effect and the chains remember their previous conformations. Then, the autocorrelation function decreases rapidly after the knot is released. This observed behavior deviates substantially from the exponential decrease predicted by the tube model.

The outer segment mean squared displacement results (in Figures 7b, 8b, and 9b) support the idea that knots are released from the chain ends. At early times, the power-law exponents (slopes of the graphs) for the outer segment mean squared displacement decrease slightly with time. Then, there is a period in which the power-law exponents remain fairly constant over time until a discontinuity occurs, and the exponents for the two lower density systems, $\phi = 0.40$ and $\phi = 0.45$, decrease significantly. Finally, at times consistent with the final relaxation of the end-to-end vector autocorrelation function, all of the systems experience a discontinuity in the power-law exponents for the outer segment mean squared displacement. At this discontinuity, the power law exponent (slope) increases dramatically. This large increase in the mobility of the outer segments indicates that considerable relaxation occurs near the chain ends at this time, which is consistent with the release of knots from chain ends.

The apparent diffusion coefficient (in Figures 7c, 8c, and 9c) can be used to locate any superdiffusive motion that could occur after the release of knots. As discussed previously, the tube model predicts that the apparent diffusion coefficient will decrease until it reaches a long-time plateau equal to the self-diffusion coefficient. However, for our systems at the lower volume fractions,

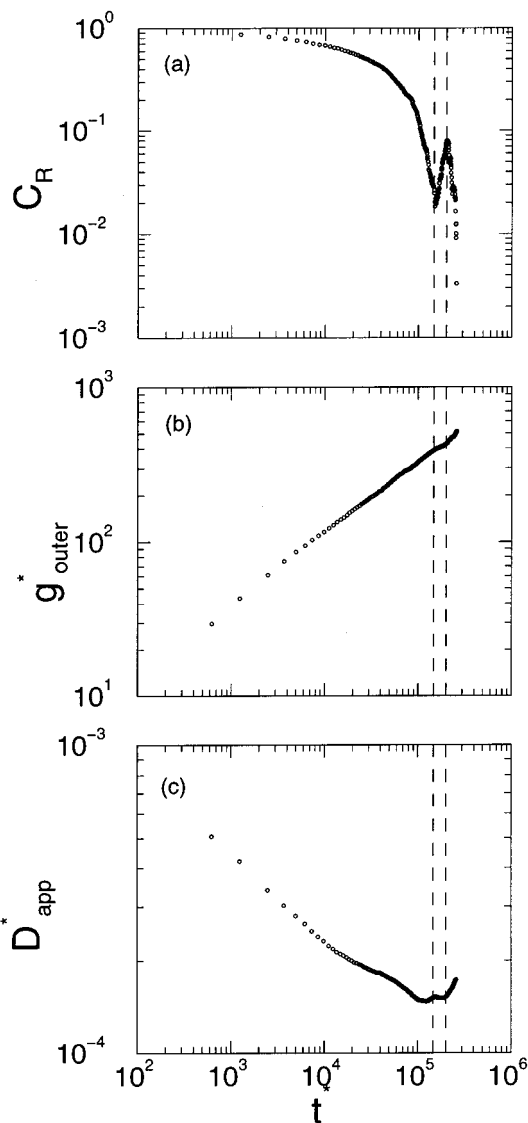


Figure 7. Simulation data for chains of length 192 at $\phi = 0.40$ displaying results consistent with knot release behavior: (a) end-to-end vector autocorrelation function, (b) outer segment mean squared displacement, and (c) apparent self-diffusion coefficient vs reduced time. The dashed lines bound the time range when knot constraints appear to affect the system.

$\phi = 0.40$ and 0.45 , the observed apparent diffusion coefficient increases at longer times, indicating superdiffusion, a center of mass mean squared displacement which scales with time to a power greater than 1. The apparent diffusion coefficient increases from the knot release time until the largest t^* by approximately 18% at $\phi = 0.40$ and 12% at $\phi = 0.45$. A significant change was not observed for the $\phi = 0.50$ system. The superdiffusive behavior may be suppressed at $\phi = 0.50$ because of the system's high density.

The error in the apparent diffusion coefficient was investigated to determine the statistical significance of the observed superdiffusive behavior. The apparent diffusion coefficient was obtained for each chain in the system to determine the sample standard deviation. The uncertainty in the system values was estimated by dividing the sample standard deviation by the square root of the sample size.⁶¹ The sample size depends on both the number of chains in the system and the percentage of the simulation time analyzed. At the total

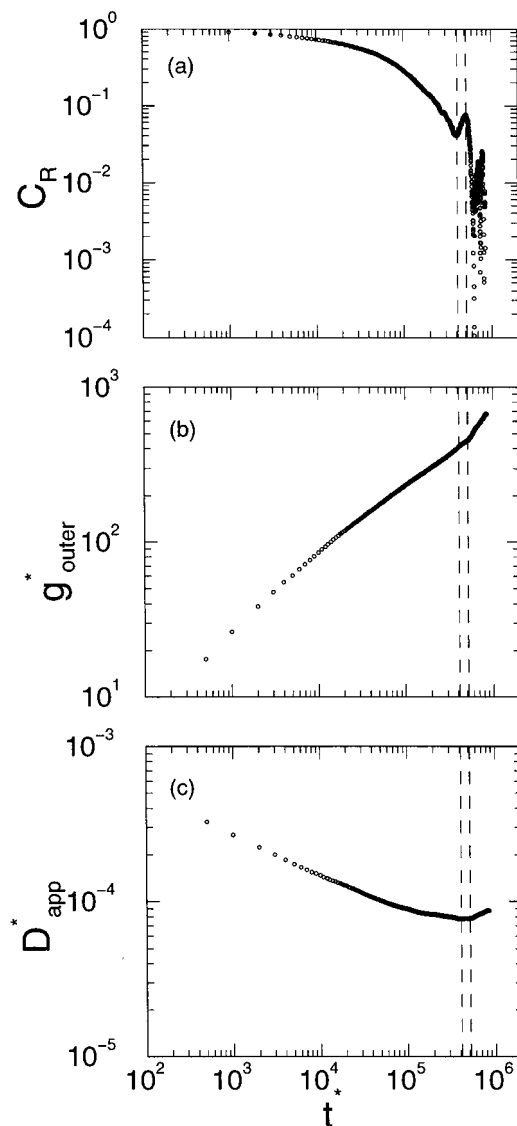


Figure 8. Simulation data for chains of length 192 at $\phi = 0.45$ displaying results consistent with knot release behavior: (a) end-to-end vector autocorrelation function, (b) outer segment mean squared displacement, and (c) apparent self-diffusion coefficient vs reduced time. The dashed lines bound the time range when knot constraints appear to affect the system.

simulation time, only one independent value is obtained for each chain in the system, thus the sample size is the number of chains. At times of 50% or less of the total simulation time, multiple independent values are obtained for each chain, such that the sample size is twice the number of chains at 50% of the total simulation time and three times the number of chains at 33% of the total simulation time. The error is largest at the longest time and decreases with decreasing time. The maximum uncertainty in the apparent diffusion coefficient at the longest times was estimated to be approximately 20% at $\phi = 0.40$ and 15% at $\phi = 0.45$, taking the sample size to be the number of chains in the system. The uncertainty at the “knot time” was estimated to be approximately 11% at $\phi = 0.40$ and 8% at $\phi = 0.45$, taking the sample size to be twice the number of chains in the system. In comparison, Kremer and Grest²² estimated that the error in their results was on the order of 10% at the longest times they reported.

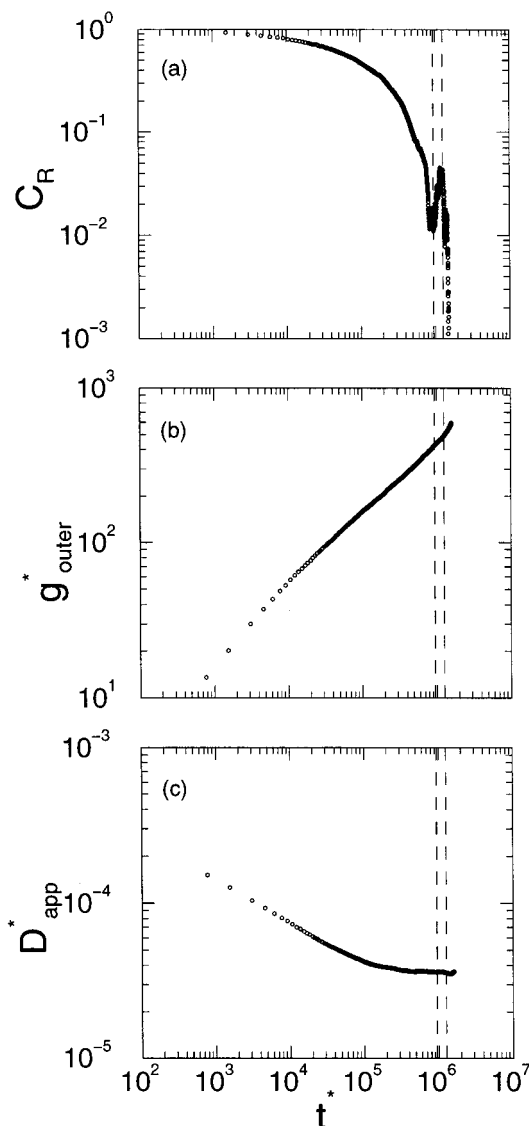


Figure 9. Simulation data for chains of length 192 at $\phi = 0.50$ displaying results consistent with knot release behavior: (a) end-to-end vector autocorrelation function, (b) outer segment mean squared displacement, and (c) apparent self-diffusion coefficient vs reduced time. The dashed lines bound the time range when knot constraints appear to affect the system.

The observed change in the apparent diffusion coefficient is on the order of the uncertainty in the values; therefore, our analysis of superdiffusive behavior must be viewed with caution. However, when considered in combination with the other quantities, the evidence is consistent with the release of interchain entanglements. The superdiffusive behavior, which is not predicted by the tube model, is observed at times consistent with the final relaxation of orientation observed in the end-to-end vector autocorrelation function and the release of the end segments obtained from the outer segment mean squared displacement. The evidence for superdiffusive behavior supports the idea that the release of interchain entanglements allows a dissipation of the energy stored during the stretching of the chains.

The release of interchain entanglements, or knots, is a discrete, localized event. Therefore, the time when it occurs is not expected to be universal. We would expect the release of knots to occur at different times for different chains within the system. If this does indeed

happen, the multiple events occurring at different times could potentially smooth out when averaging over more data. Thus, the plateaus and bumps witnessed in the correlation functions may not still be visible at the same times if the simulations are run for much longer or if the system size is increased dramatically. They might move to later times or smooth out altogether. Our observations are consistent with the presence and release of interchain entanglements and knots but not at a universal time. Because our three starting configurations at different volume fractions were obtained from the same initial configuration at $\phi = 0.28$ (prior to growing and equilibration), many of the long time features will be similar. Therefore, we believe that the three different knot release times obtained at the three different volume fractions can be compared to each other to determine the effect of density on the time it takes knots to release.

A comparison of the results from the different density systems reveals that both the duration of knot constraints and the time of knot release increase with increasing volume fraction, or density. Interchain entanglement constraints occurred over the following time ranges: $149\,000 \leq t^* \leq 202\,000$ for $\phi = 0.40$, $414\,000 \leq t^* \leq 519\,000$ for $\phi = 0.45$, and $952\,000 \leq t^* \leq 1\,275\,000$ for $\phi = 0.50$. These time ranges which are indicated by dashed lines in the figures were determined from the end-to-end vector autocorrelation functions, as displayed in Figures 7a, 8a, and 9a. The time when C_R begins to increase is estimated to be the onset of knot constraints, and the time when C_R begins to decrease again is estimated to be the knot release time. These times and the range between them increase with increasing volume fraction.

Although higher densities increase the time and duration of knot release, they diminish the effect of knot release by prohibiting the released chains from moving very far. This is supported by the fact that the changes in both the outer segment mean squared displacement and the apparent diffusion coefficient results that accompany knot release diminish with increasing volume fraction. The two lowest density systems studied exhibit a decrease in the outer segment mean squared displacement's power law exponent over the duration of the knot constraints. However, the exponent of the highest density system, $\phi = 0.50$, does not experience a significant change during this time. At the knot release time, the outer segment mean squared displacement of all three systems undergoes a dramatic increase in its power law exponent with time. The power law exponent of the $\phi = 0.50$ system's outer segment mean squared displacement does not experience as dramatic of an increase as that of the lower density systems, since its outer segment mean squared displacement exponent had not decreased much during the knot constraint time. In the two lowest density systems, the apparent diffusion coefficient displays superdiffusive behavior immediately following the time of knot release. However, this analysis is made with caution, because the observed change in the apparent diffusion coefficient is on the order of the uncertainty in the values. The apparent diffusion coefficient of the $\phi = 0.50$ system does not increase like that of the other, less-dense systems. The much higher density of the $\phi = 0.50$ system may prohibit the chains from moving quickly to a more favorable conformation when a knot is released.

V. Conclusions

In this study, discontinuous molecular dynamics simulations were performed to investigate entanglement relaxation and release in model polymer melts. The relaxation behavior was first compared to that predicted by the tube model which dictates that chain relaxation begins at the chain ends and progresses inward until the chain middle relaxes at the final relaxation time. Then, the simulation results were analyzed in light of a proposed mechanism for interchain entanglement or knot release, consisting of initial relaxation, followed by memory and final release from a chain end.

To compare the simulation results to the tube model, the model's three relaxation times, τ_e , τ_R , and τ_d , were estimated for all of the systems studied. Three different methods for determining the longest relaxation time, τ_d , as prescribed by the tube model, provided inconsistent results, thus identifying a discrepancy between the simulation results and the tube model.

To investigate the inconsistency of the τ_d estimates, the mean squared displacements of the chain center of mass and chain segments at various positions along the chain (including inner segments in the chain middle, intermediate segments along the chain, and outer segments at the chain ends) were studied. These mean squared displacements revealed that at early times, chain relaxation begins at the outer segments and continues inward along the chain. However, this trend does not continue throughout time, and final relaxation does not occur at the segments in the chain middle but instead is observed at the outer segments. The actual final relaxation of the systems, as determined from the mean squared displacement behavior, occurred at times which were longer than the first two τ_d predictions obtained using tube model methods. Therefore, it was determined that another method of entanglement release was present in the simulation systems.

A proposed mechanism of interchain entanglement release was described which provides a physical picture of the observed relaxation behavior. This mechanism for interchain entanglement, or knot, release consists of three stages in time, initial chain relaxation, memory of previous conformations, and final release of the knot from a chain end. The initial chain relaxation was observed as a decrease of the end-to-end vector autocorrelation function. Memory of previous conformations was associated with an increase in the end-to-end vector autocorrelation function. The release from a chain end was reflected in an increased power law exponent in the outer segment mean squared displacement results. The superdiffusion experienced by the released chains of the two lowest density systems is consistent with an increase in the apparent diffusion coefficient immediately following the knot release although this change was on the order of the uncertainty in the values. A combined analysis of the end-to-end vector autocorrelation function, the outer segment mean squared displacement, and the apparent diffusion coefficient was used to determine the duration and time of knot release. Although, the knot release times are not universal, the values obtained for the different density systems could be compared to each other since each system was obtained from a single initial configuration at $\phi = 0.28$ (prior to growing and equilibration). It was found that both the duration of knot constraints and the time of knot release increased with increasing volume fraction. However, the dramatic effect of the knot release on the

outer segment mean squared displacement and the apparent diffusion coefficient diminished with increasing volume fraction indicating that higher density prohibits the released chains from moving very far. Because the proposed knot release behavior occurred over long times where the statistical error is largest, this should be interpreted with caution.

This study adds to our knowledge and understanding of entanglement relaxation and release. In so doing, it provides additional information about the nature of entanglements and suggests areas for further study. The results from this study indicate that the release of interchain entanglements, or knots, is a significant contribution to entanglement relaxation. This suggests that localized behavior should be studied in greater depth.

Acknowledgment. This work was supported by a National Science Foundation Graduate Research Fellowship, a DuPont Graduate Fellowship, an Eastman Graduate Fellowship, and the Office of Energy Research, Basic Sciences, Chemical Science Division of the U.S. Department of Energy under Contract Number DE-FG02-97-ER14771. Acknowledgment is made to the donors of the Petroleum Research Fund administered by the American Chemical Society for partial support of this work. We thank the North Carolina Supercomputing Center for grants of computer time and file storage space.

References and Notes

- Lodge, T. P.; Rotstein, N. A.; Prager, S. In *Advances in Chemical Physics*; Prigogine, I., Rice, S. A., Eds. Interscience: New York, 1990.
- Szamel, G.; Wang, T. *J. Chem. Phys.* **1997**, *107*, 10793.
- de Gennes, P. G. *J. Chem. Phys.* **1971**, *55*, 572.
- Doi, M.; Edwards, S. F. *J. Chem. Soc., Faraday Trans. 2* **1978**, *74*, 1789.
- Iwata, K.; Edwards, S. F. *Macromolecules* **1988**, *21*, 2901.
- Iwata, K.; Edwards, S. F. *J. Chem. Phys.* **1989**, *90*, 4567.
- des Cloizeaux, J. *Europhysics Lett.* **1988**, *5*, 437.
- des Cloizeaux, J. *Macromolecules* **1992**, *25*, 835.
- des Cloizeaux, J. *J. Phys. I Fr.* **1993**, *3* (1), 61.
- des Cloizeaux, J. *Macromol. Symp.* **1994**, *81*, 1.
- Smith, S. W.; Hall, C. K.; Freeman, B. D. *J. Chem. Phys.* **1996**, *104*, 5616.
- Ewen, B.; Richter, D. *Adv. Polym. Phys.* **1997**, *134*, 1.
- Schleger, P.; Farago, B.; Lartigue, C.; Kollmar, A.; Richter, D. *Phys. Rev. Lett.* **1998**, *81*, 124.
- Komlosh, M. E.; Callaghan, P. T. *J. Chem. Phys.* **1998**, *109*, 10053.
- Skolnick, J.; Kolinski, A.; Yaris, R. *Acc. Chem. Res.* **1987**, *20*, 350.
- Kolinski, A.; Skolnick, J.; Yaris, R. *J. Chem. Phys.* **1987**, *86*, 1567.
- Kolinski, A.; Skolnick, J.; Yaris, R. *J. Chem. Phys.* **1987**, *86*, 7164.
- Skolnick, J.; Kolinski, A. *Adv. Chem. Phys.* **1990**, *78*, 223.
- Paul, W.; Binder, K.; Heermann, D. W.; Kremer, K. *J. Chem. Phys.* **1991**, *95*, 7726.
- Binder, K.; Paul, W. *J. Polym. Sci., B: Polym. Phys.* **1997**, *35*, 1.
- Kreer, T.; Baschnagel, J.; Müller, M.; Binder, K. *Macromolecules* **2001**, *34*, 1105.
- Kremer, K.; Grest, G. S. *J. Chem. Phys.* **1990**, *92*, 5057.
- Dunweg, B.; Grest, G. S.; Kremer, K. In *The IMA Volumes in Mathematics and its Applications*; Whittington, S. G., Ed.; Springer-Verlag: New York, 1998; Vol. 102, p 159.
- Pütz, M.; Kremer, K.; Grest, G. S. *Europhys. Lett.* **2000**, *49*, 735.
- Smith, S. W.; Hall, C. K.; Freeman, B. D. *Phys. Rev. Lett.* **1995**, *75*, 1316.
- Smith, S. W.; Hall, C. K.; Freeman, B. D.; McCormick, J. A. In *The IMA Volumes in Mathematics and its Applications*; Whittington, S. G., Ed.; Springer-Verlag: New York, 1998; Vol. 102, p 203.
- Doi, M.; Edwards, S. F. *The Theory of Polymer Dynamics*; Clarendon: Oxford, England, 1986.
- Berry, G. C.; Fox, T. G. *Adv. Polym. Sci.* **1968**, *5*, 261.
- Lodge, T. P. *Phys. Rev. Lett.* **1999**, *83*, 3218.
- Tao, H.; Lodge, T. P.; von Meerwall, E. D. *Macromolecules* **2000**, *33*, 1747.
- Skolnick, J.; Yaris, R.; Kolinski, A. *J. Chem. Phys.* **1988**, *88*, 1407.
- Müller, M.; Wittmer, J.; Cates, M. *Phys. Rev. E* **1996**, *53*, 5063.
- Gao, J.; Weiner, J. H. *J. Chem. Phys.* **1995**, *103*, 1621.
- Ben-Naim, E.; Grest, G. S.; Witten, T. A.; Balijon, A. R. C. *Phys. Rev. E* **1996**, *53*, 1816.
- Kolinski, A.; Skolnick, J. *J. Phys. Chem.* **1993**, *97*, 3450.
- Schweizer, K. S. *J. Chem. Phys.* **1989**, *91*, 5802.
- Schweizer, K. S. *J. Chem. Phys.* **1989**, *91*, 5822.
- Smith, S. W.; Hall, C. K.; Freeman, B. D. *J. Comput. Phys.* **1997**, *134*, 16.
- Trautenberg, H. L.; Wittkop, M.; Goritz, D. *Phys. Rev. Lett.* **1996**, *76*, 4448.
- Smith, S. W.; Hall, C. K.; Freeman, B. D. *Phys. Rev. Lett.* **1996**, *76*, 4449.
- Flory, P. J. *Statistical Mechanics of Chain Molecules*; Interscience: New York, 1969.
- Rapaport, D. C. *J. Phys. A: Math. Gen.* **1978**, *11*, L213.
- Bellemans, A.; Orban, J.; Belle, D. V. *Mol. Phys.* **1980**, *39*, 781.
- Alder, B. J.; Wainwright, T. E. In *Symposium on Transport Processes In Statistical Mechanics*; Prigogine, I., Ed.; Interscience: New York, 1956.
- Alder, B. J.; Wainwright, T. E. *J. Chem. Phys.* **1959**, *31*, 459.
- Haile, J. M. *Molecular Dynamics Simulation: Elementary Methods*; Wiley: New York, 1992.
- Allen, M. P.; Tildesley, D. J. *Computer Simulation of Liquids*; Clarendon: Oxford, England, 1987.
- Rapaport, D. C. *J. Comput. Phys.* **1980**, *34*, 184.
- Erpenbeck, J. J.; Wood, W. W. In *Modern Theoretical Chemistry*; Berne, B. J., Ed.; Plenum: New York, 1977; Vol. 6, p 1.
- Zhou, Y.; Smith, S. W.; Hall, C. K. *Mol. Phys.* **1995**, *86*, 1157.
- Einstein, A. *Ann. Phys. (Leipzig)* **1901**, *17*, 549.
- Einstein, A. *Investigations on the Theory of Brownian Movement*; Dover: New York, 1956.
- Doi, M. *J. Polym. Sci.: Polymer Lett. Ed.* **1981**, *19*, 265.
- Doi, M. *J. Polym. Sci.: Polym. Phys. Ed.* **1983**, *21*, 667.
- Milner, S.; McLeish, T. *Phys. Rev. Lett.* **1998**, *81*, 725.
- Frischknecht, A. L.; Milner, S. T. *Macromolecules* **2000**, *33*, 5273.
- de Gennes, P. G. *Macromolecules* **1976**, *9*, 587, 594.
- Klein, J. *Macromolecules* **1978**, *11*, 852.
- Dauod, M.; deGennes, P. G. *J. Polym. Sci.: Polym. Phys. Ed.* **1979**, *17*, 1971.
- Graessley, W. W. *Adv. Polym. Phys.* **1982**, *47*, 67.
- Hogg, R. V.; Ledolter, J. *Applied Statistics for Engineers and Physical Scientists*; Macmillan Publishing Co.: New York, 1992; Chapter 4.